

Full length article

Pump-driven wavelength switching in an all-polarization-maintaining mode-locked fiber laser incorporating a CNT/PDMS saturable absorber

Maolin Dai^{a,b}, Bowen Liu^{a,b}, Guanyu Ye^{a,b}, Takuma Shirahata^{a,b}, Yifan Ma^{a,b}, Naoki Yamaguchi^{a,b}, Sze Yun Set^{a,b,*}, Shinji Yamashita^{a,b}

^a Department of Electrical Engineering and Information Systems (EEIS), The University of Tokyo, Bunkyo-ku, Tokyo 113-8656, Japan

^b Research Center for Advanced Science and Technology (RCAST), The University of Tokyo, Meguro-ku, Tokyo 153-8904, Japan



ARTICLE INFO

Keywords:

Ultrafast fiber lasers
Passive mode-locking
Carbon nanotubes
All-polarization-maintaining
Wavelength tuning
Dual-wavelength mode-locking
Intracavity loss
Reverse saturable absorption
Optical limiting

ABSTRACT

Mode-locked fiber lasers with wavelength tunability and dual-wavelength mode-locking capability have wide applications in nonlinear imaging, precision metrology and photonic sensing. Here, for the first time, we propose and experimentally demonstrate an environmentally stable all-polarization-maintaining (all-PM) fiber mode-locked laser without any intracavity filter and attenuator, whose mode-locking wavelength is switchable with the injected pump power. By increasing the pump power, the mode-locking wavelength switches from 1560-nm band to 1560/1530-nm dual-wavelength mode-locking, and finally to the 1530-nm band. The mechanism behind the phenomenon is well explained by the reverse saturable absorption induced intracavity loss variation. The proposed laser has a very concise configuration with only one integrated wavelength-division-multiplexer and a carbon nanotubes/polydimethylsiloxane (CNT/PDMS) saturable absorber (SA). The compact size, simple wavelength switching scheme as well as environmental stability makes it promising for practical applications.

1. Introduction

Ultrafast fiber lasers, especially passively mode-locked fiber lasers delivering picosecond (ps) or femtosecond (fs) optical pulses have been widely adopted in various applications, from fundamental research to industry scenarios, with compact size, high energy transferring efficiency, and high stability [1–3]. From a historical perspective, various mode-locking methods have been developed since the 1990's. In passively mode-locked fiber lasers, real saturable absorbers (SAs) based on nanomaterials or artificial SAs based on nonlinear fiber optics are employed to filter out the low intensity optical component to form high peak-power short pulses.

The common artificial SAs used in current mode-locked fiber laser systems include nonlinear polarization evolution (NPE) [4–6], nonlinear optical loop mirror (NOLM) [7,8], and nonlinear amplifying loop mirror (NALM) [9–11]. For NPE lasers, most of them are built with non-polarization-maintaining (non-PM) optical fibers, because of the intrinsic polarization dependent pulse picking mechanism. In recent years, some works have achieved the NPE mode-locking with all-PM fibers, nevertheless their strict working conditions [12–14]. NOLM and NALM are all-PM compatible, however, a non-reciprocal phase

shifter should be added to make the laser self-starting [15,16]. In the contrast, in recent years, the real SAs are widely used for ultrafast fiber laser mode-locking owing to their excellent saturable absorption properties, including semiconductor saturable absorber mirrors (SESAMs) [17,18], carbon nanotubes (CNTs) [19,20], graphene [21,22], topological insulators (TIs) [23,24], transition metal dichalcogenides (TMDs) [25,26], black phosphorus (BP) [27,28], MXene [29–31] and many others [32–36]. These real SAs are low-cost, easy-fabrication, PM-fiber compatible, and allow the pulsed laser self-starting. Especially, CNT-SA has been widely adopted for realizing ultrashort pulse generation in various kinds of cavities since its first demonstration.

Mode-locked fiber lasers with wavelength tunability/switchability and multiwavelength mode-locking capability enable promising applications in biochemical sensing, imaging and precise spectroscopy. For Er-doped fiber (EDF) lasers, the wavelength tuning range is limited in C-band, which covers 1530 nm to 1560 nm, owing to the gain emission profile. Typically, a fiber or free-space wavelength filter is inserted into the laser cavity to pick up the operating wavelength. Recently, PM-fiber based Lyot filter shows its potential as a favorable candidate with free spectral range (FSR) tunability for realizing such function by actively picking up the desirable wavelengths [37,38]. Another common method

* Corresponding author.

E-mail addresses: maolin@cntp.t.u-tokyo.ac.jp (M. Dai), set@cntp.t.u-tokyo.ac.jp (S.Y. Set).

<https://doi.org/10.1016/j.optlastec.2024.111002>

Received 5 December 2023; Received in revised form 13 March 2024; Accepted 8 April 2024

Available online 17 April 2024

0030-3992/© 2024 Published by Elsevier Ltd.

for realizing dual-wavelength mode-locking in both 1530-nm band and 1560-nm band, is employing two independent laser oscillators in the same laser configuration by using two wavelength division multiplexers (WDMs) for both two bands [39,40]. The proposed laser has two main resonant loops for oscillating two different wavelength components simultaneously, while the gain fiber and SA are shared in the common path. Except for above-mentioned two approaches, there is another possibility to employ an optical attenuator for the realization of dual-wavelength mode-locking in the 1530- and the 1560-nm band by making use of the intrinsic gain curve of the EDF. Following this principle, researchers have realized switchable single-wavelength and dual-wavelength mode-locking by tuning an intracavity optical attenuator [41–43]. In this case, the filter is not a necessity, the wavelength switching as well as gain equalization is totally dependent on the intracavity power. However, the realization of wavelength switching is based on an optical attenuator which is slow and bulky, and the laser is constructed with non-PM fibers, making it highly susceptible to environmental disturbance.

Here, in this paper, for the first time, we achieve pump-power-controlled wavelength switching in a concise all-PM Er-doped mode-locked fiber. The mode-locking is realized by using a CNT/Polydimethylsiloxane (PDMS) SA. The operating wavelength of this laser can be switched between 1560-nm band, 1530-nm band, and 1560/1530-nm dual wavelength bands, without losing its mode-locking. There is no intracavity filter or attenuator to equalize the gain/loss, the wavelength switching is totally dependent on the injected pump power. The mechanism behind the phenomenon is reasonably explained by the reverse saturable absorption of the SA. By using an all-PM fiber configuration, the laser's robustness can be guaranteed. The proposed laser is promising for biochemical sensing, imaging with extended wavelength window, and wavelength multiplexed dual comb spectroscopy.

2. Experiment setup

The experimental setup is shown in Fig. 1. In the laser oscillator, we use a compact PM tap-isolator-wavelength-division-multiplexer (PM-TIWM) hybrid device which functions as a 10 % output coupler, an isolator and a WDM. PM Er-doped fiber of 80-cm in length (PM-EDF, Nufern PM-ESF-7/125) with a group velocity dispersion (GVD) of $-20 \text{ fs}^2/\text{mm}$ and a core absorption of $55.0 \pm 5.0 \text{ dB/m}$ near 1530 nm is used as the gain medium, pumped by a 980-nm laser diode (LD, 3SP

Technologies, 1999CHB). The laser is mode-locked using a SA consisting of a CNT/PDMS film, sandwiched between two fiber connectors. The other part of the oscillator is the single-mode PMF with a GVD of $-22.9 \text{ fs}^2/\text{mm}$ to complete a 7.2-m laser cavity. Therefore, the total intracavity dispersion is calculated to be -0.16 ps^2 . The insets (i) and (ii) in Fig. 1 show the photos of the CNT/PDMS-SA from different perspectives. In the experiment, the optical spectrum is measured using an optical spectrum analyzer (OSA, YOKOGAWA, AQ6370D). The optoelectronic conversion is realized using a 1-GHz photodetector (NEWFOCUS 1611). The time-domain pulse train and radiofrequency (RF) spectrum are recorded by an oscilloscope (RIGOL DS2202A) and an electrical frequency analyzer (ESA, RIGOL, RSA3045), respectively. The autocorrelation (AC) trace of the optical pulse is measured by an autocorrelator (Femtochrome, FR-103XL).

The preparation process of the CNT/PDMS-SA is modified based on the reported method in Ref. [44]. First, high-pressure carbon monoxide (HiPco)-synthesized single-wall CNT powder (NanoIntegris) with diameter of 0.8–1.2 nm is added into isopropyl alcohol (IPA) of 100 mL, and the mixture is fully dispersed by an ultrasonic processor. After a 30-minute ultrasonication, the solution appears black and semi-transparent. A small amount of methyl group-terminated PDMS (MEP), which is low in viscosity ($50 \text{ mm}^2/\text{s}$), is then added and dispersed within the CNT/IPA solution using ultrasonication. This step enhances the bonding between CNT and PDMS. Subsequently, PDMS-A, the silicone elastomer base, is mixed into the CNT/IPA/MEP solution in the same manner. The next step involves removing the IPA from the solution by heating the CNT/IPA/MEP mixture to $80 \text{ }^\circ\text{C}$ under magnetic stirring. After 6 h, once the IPA is fully evaporated, PDMS-B, the curing agent, is added to the beaker at room temperature with a weight ratio of 10:1 (PDMS-A: PDMS-B), and the mixture is stirred magnetically. Finally, the thoroughly mixed CNT/PDMS solution is poured into a cell, and a thin film is formed using a spin coater. The CNT/PDMS film is then placed in a thermostat for solidification, under $50 \text{ }^\circ\text{C}$ circumstance. After 48 h, small pieces of the fully solidified CNT/PDMS film with micrometer-level thickness are applied to the fiber connector to serve as SAs.

3. Experimental results and discussions

3.1. Single-wavelength mode-locking

Different from previous works [42,43], the wavelength switching in our proposed mode-locked laser does not rely on an external optical filter, attenuator or birefringent filtering effect. The operating wavelength switching and dual-wavelength mode-locking operations can be realized solely by tuning the pump power, since the gain spectral profile of the EDF is different when under different pump power, induced by the intracavity loss variation, which we will explain in the discussion part. Specifically, when under lower pump power, the peak emission wavelength at 1560 nm will be dominant, while higher pump power will shift the emission peak to near 1530 nm.

In the experimental demonstration, we inject different pump power to our laser oscillator, and record the laser output. When the pump power is increased to 40 mW, self-started mode-locking is easily achieved, benefiting from the high performance of the CNT/PDMS-SA. The pump power is slightly reduced to 35 mW, close to the mode-locking threshold to keep a stable single-pulse state. The measured output power is about 0.25 mW. The output optical spectrum is shown in Fig. 2 (a). With a relatively low pump power injection, the central wavelength of mode-locking is located at 1558.9 nm and the full-width-at-half-maximum (FWHM) is measured as 2.7 nm. Weak Kelly sidebands locating at both sides of the laser center wavelength can be observed. The oscilloscope trace of the output pulse train is shown in a 500-ns temporal window as shown in Fig. 2(b), where a clear and even pulse train with an interval of $\sim 35 \text{ ns}$ is observed, confirming the single-pulse operation. The RF spectrum is shown in Fig. 2(c). The frequency spectra

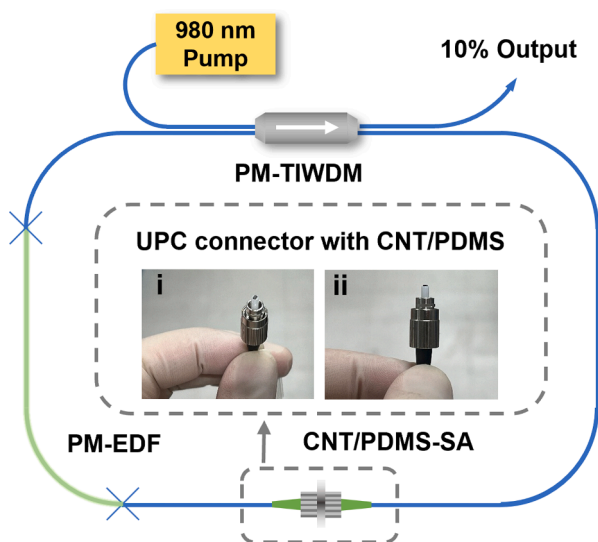


Fig. 1. Experiment setup of the all-PM mode-locked fiber laser. TIWM: tap-isolator-wavelength-division-multiplexer; EDF: Er-doped fiber.

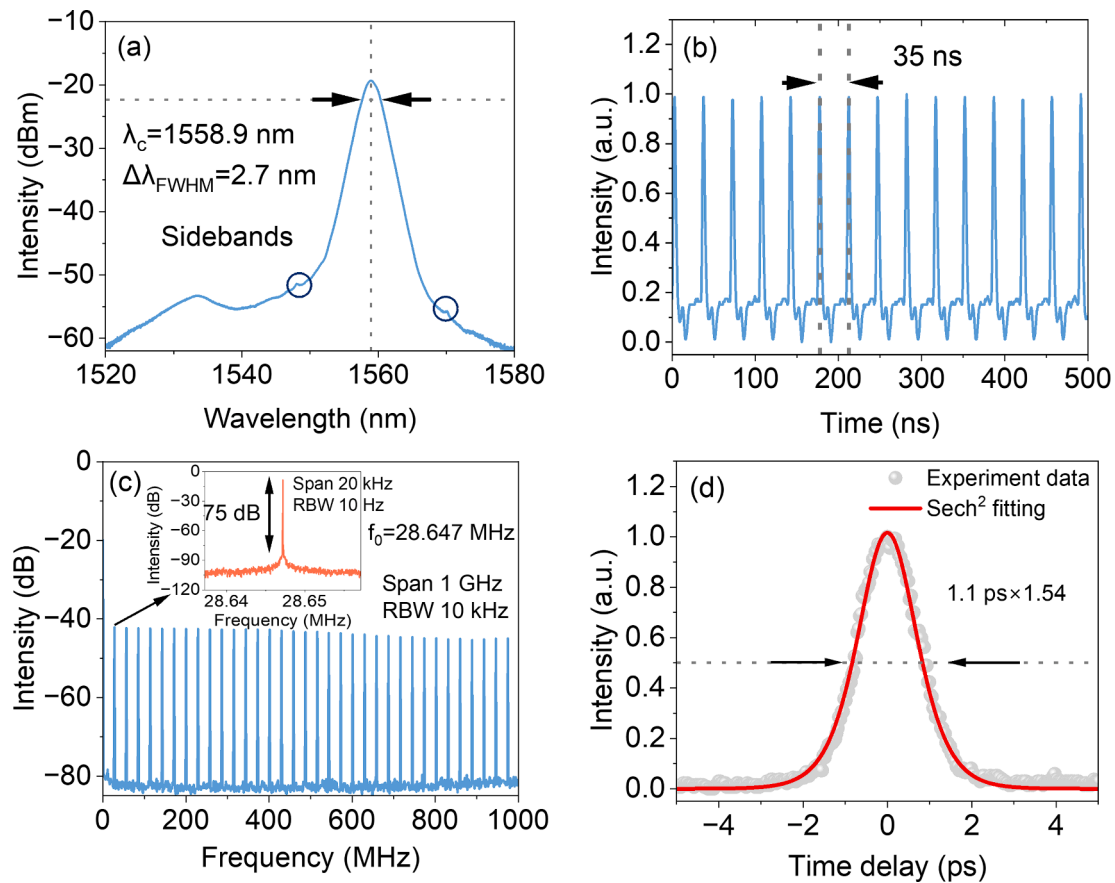


Fig. 2. Measured results of the mode-locked fiber lasers when operating at the center wavelength of 1558.9 nm with pump power of 35 mW. (a) Optical spectrum, (b) pulse trains, (c) RF spectra in 1-GHz span and in 20-kHz span, and (d) AC trace.

in a 1-GHz span with a resolution bandwidth (RBW) of 10 kHz and in a 20-kHz span with a RBW of 10 Hz are shown in the graph and its inset, respectively. The first-order frequency is located at 28.647 MHz, denoting that the laser owns a fundamental repetition rate of this value, which is well consistent with the abovementioned pulse interval and the cavity length of 7.2 m. The high signal-to-noise ratio (SNR) of > 75 dB proves the robustness of laser mode-locking. The AC trace recorded is shown in Fig. 2(d). The pulse duration is measured as 1.1 ps, with a time-bandwidth product (TBP) of 0.366, which is slightly higher than that of the transform limited pulse. The picosecond pulse width may result from many factors, such as intracavity dispersion, modulation depth of SA, and low pump power we injected. Shorter pulse width can be obtained by increasing the pump power to enhance the nonlinear pulse compression or using a SA with higher modulation depth [45,46]. For The AC trace is well fitted by the sech^2 fitting, proving that the optical pulse is a conventional soliton, as expected from an all-anomalous-dispersion laser cavity.

Then we turn up the pump power to around 100 mW, the mode-locking with a 3-dB bandwidth of 2.3 nm and a center wavelength of 1532.6 nm is obtained, whose optical spectrum is shown in Fig. 3(a). The measured output power is 1.9 mW. There exists some amplified spontaneous emission (ASE) noise in 1560-nm band. In Fig. 3(b), the pulse train has an interval of 35 ns, almost the same as that of 1560-nm band mode-locking. The RF spectra in Fig. 3(c) shows the laser's repetition rate is around 28.649 MHz, which is ~ 2 kHz higher than when operating at 1560-nm band due to the group velocity dispersion in the cavity. The AC trace shown in Fig. 3(d) represents the laser pulse in the cavity, which shows laser pulse owns a duration of 1.4 ps. The duration is wider than when mode-locked at 1560-nm band, the main reason is that the EDF has a narrow emission spectral width in 1530-nm band. This result

is also consistent with other previous works [43]. The calculated TBP is about 0.41, which shows the optical pulse has a slight chirp. The 2-m single mode fiber outside the cavity when measuring the AC trace also contributes to broadening the pulse width.

3.2. Dual-wavelength mode-locking and wavelength switching

As the gain profile transfer is a gradual process, under a certain pump power range, the gain levels in the two bands are close, making it possible for a dual-wavelength mode-locking. When the pump power is in the range of 80–100 mW, dual-wavelength mode-locking is manifested. The measured optical spectrum and RF spectrum with 10-Hz RBW when pumped at 90-mW power are shown in Fig. 4(a) and (b), respectively. The center wavelengths of the dual-wavelength mode-locked pulses are 1532.6 nm and 1554.9 nm, with the 3-dB bandwidths of 2.4 nm and 4.6 nm, respectively. The optical spectrum is much broader than that of the single-wavelength mode-locking at the 1560-nm band owing to the wide emission spectral gain bandwidth under a high pump power. The strong Kelly sidebands are explicitly observed in both sides of the 1554.9-nm output peak, caused by the high intracavity power. It is noted that, when the dual-wavelength mode-locking is built up, the mode-locking of longer wavelength is in multi-pulse state due to the soliton area theorem. However, owing to the instrument limitations, we don't have tunable bandpass filters with low insertion loss to measure the individual AC trace for two mode-locked wavelengths.

The RF spectrum clearly shows the repetition rate difference between the two pulse trains, which is 2.4 kHz. Given the dispersion of ~ 16 ps/nm/km for PM Er-doped fiber [47] and ~ 18 ps/nm/km for passive PM fiber [48], the average chromatic dispersion D_{ave} is calculated as 17.8 ps/nm/km. The repetition rate difference Δf_r is calculated as $\Delta f_r =$

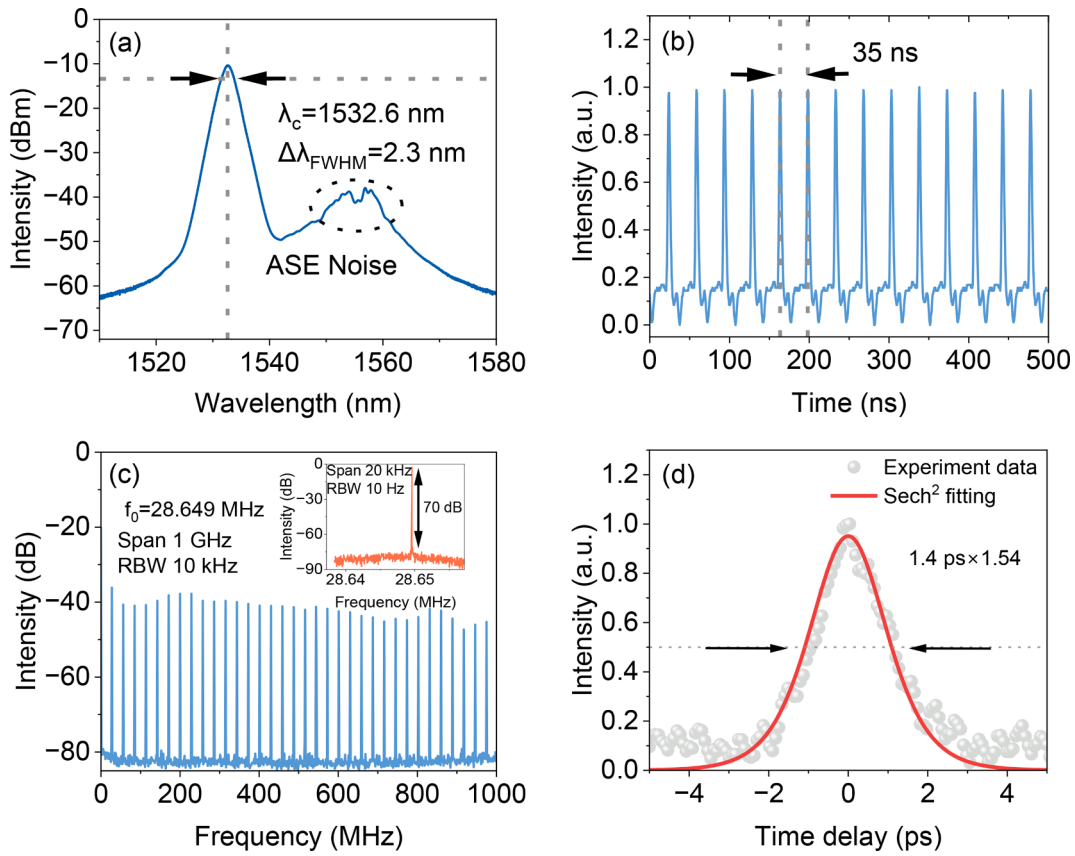


Fig. 3. Measured results of the mode-locked fiber lasers when operating at the center wavelength of 1532.6 nm with pump power of 100 mW. (a) Optical spectrum, (b) pulse trains, (c) RF spectra in 1-GHz span and in 20-kHz span, and (d) AC trace.

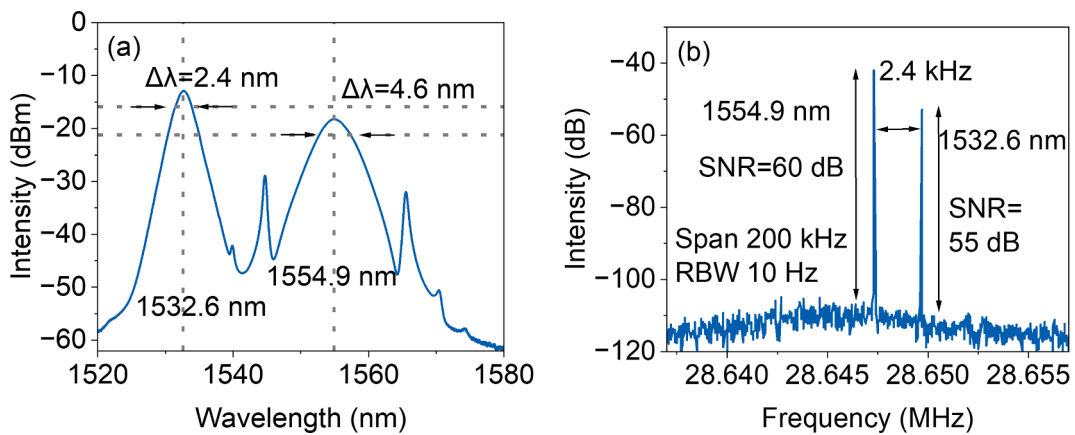


Fig. 4. Measured results of dual-wavelength mode-locking at 1532.6 nm and 1554.9 nm, when pump power is 90 mW. (a) Optical spectrum, (b) RF spectrum.

$f_r^2 D_{ave} L \Delta \lambda$ [49], where f_r is the repetition rate of the laser cavity, L is the cavity length, $\Delta \lambda$ is the wavelength difference between two mode-locked components. The measured data (2.4 kHz) is well consistent with the calculated value (2.35 kHz), the small deviation may result from the parameter error of the optical fibers. The SNRs are measured as 60 dB and 55 dB for long-wavelength and short-wavelength optical pulses, respectively, showing the robustness of the dual-wavelength mode-locking operation.

To assess the operation stability of dual-wavelength mode-locking, we record the evolution of laser’s optical spectrum and output power for 2 h. The optical spectrum is measured every minute with a resolution of 0.1 nm using the OSA, and the output power of the laser is measured every 100 ms using an optical power meter (Thorlabs, PM-400). It is

noted that no active or passive protection on the laser is used during the stability test. The results are shown in Fig. 5(a) and Fig. 5(b), respectively. In the testing period, the optical spectrum has no noticeable changes in its spectral shape and intensity, showing the robustness operation of the mode-locking. The average output power is measured as 1.5 mW, with a fluctuation of 0.04 mW and standard deviation of 0.0087 mW. The variance coefficient is calculated as 0.58 %, indicating a good stability of the laser output.

Fig. 6(a) shows the mode-locking transition process. When we continuously tune the pump power from low to high. The single-wavelength mode-locking at 1560 nm band, dual-wavelength mode-locking at both 1560 nm and 1530 nm, and single-wavelength mode-locking at 1530 nm band are achieved subsequently, corresponding to

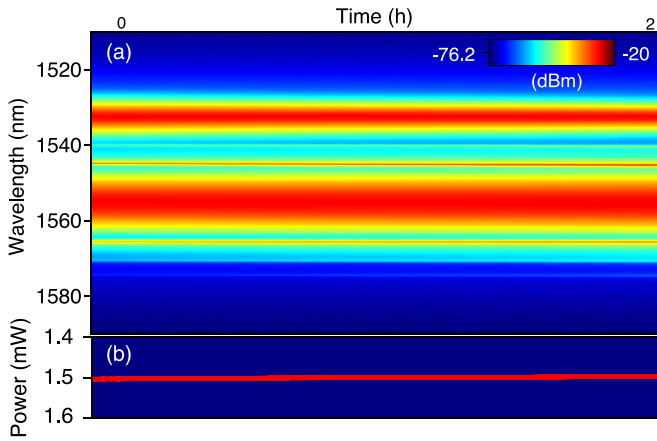


Fig. 5. Operation stability of dual-wavelength mode-locking in 2 hours. (a) Optical spectrum, (b) output power.

area (i), (ii), and (iii), respectively. It is clear that, with the increase of pump power, the Kelly sidebands enhances obviously, because of the enhanced constructive interference of the dispersive waves [50]. In Fig. 6(b), the blue dots are the measured data of output power with the increased pump power. The regions A to G, represent non-mode-locking (<30 mW), 1560-nm mode-locking (30–50 mW), multi-pulse state (50 – 85 mW), dual-wavelength mode-locking (85 – 100 mW), multi-pulse state (100 – 105 mW), 1530-nm mode-locking (105 – 115 mW), multi-pulse state (>115 mW), respectively. The red dashed line shown in Fig. 6(b) is the linear fitting curve of the data in low pump power region (30 – 70 mW). Obviously, the real output power deviates from the expectant curve, which has an efficiency slope of 2.7%. This is caused by optical limiting effect, which can arise from the reverse saturable absorption, nonlinear refraction, nonlinear scattering and mismatched indices [51]. In the next section, we demonstrate the optical limiting in our work is attributed to reverse saturable absorption, which is also the reason for pump-driven mode-locking switching.

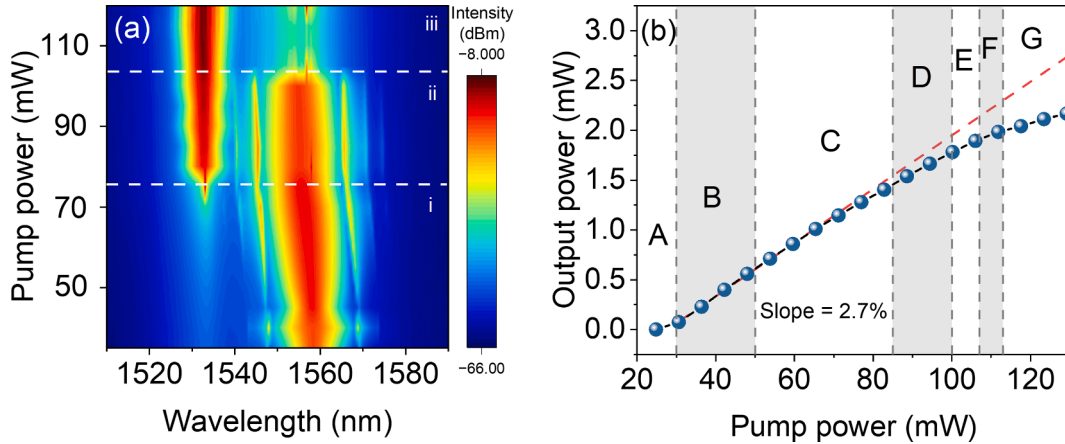


Fig. 6. Tuning of the mode-locking states from 1558.9 nm to 1532.6 nm, including dual-wavelength mode-locking when gradually increase the pump power. (a) Optical spectrum evolution map, and (b) different operation regimes and output power versus pump power.

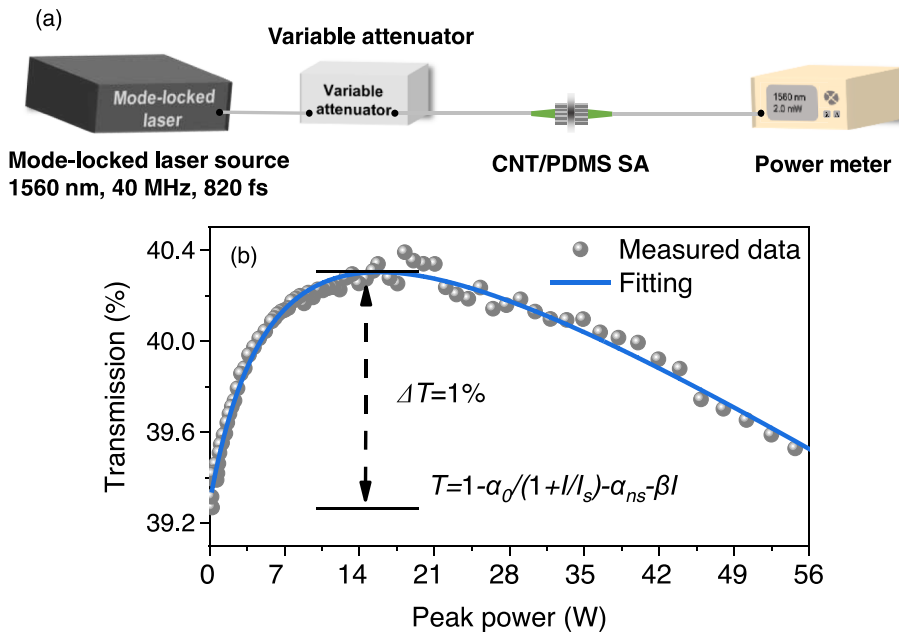


Fig. 7. Schematic diagram of the experiment setup for measuring the nonlinear saturable absorption of the CNT/PDMS. (b) Measured result and fitting curve.

3.3. Reasons for pump-driven mode-locking switching

To explain the intrinsic mechanism behind the phenomenon of pump-driven mode-locking switching and optical limiting in such a concise all-PM laser cavity, the transmission characteristics of CNT/PDMS-SA are measured. The schematic diagram of experiment setup is shown in Fig. 7(a). A commercialized femtosecond laser (AlnairLabs, PFL-200) with a center wavelength of 1558 nm, pulse width of 820 fs and repetition rate of 40 MHz is used as the light source, an optical variable attenuator (Hewlett Packard, 8156A) is used for controlling the optical power launching into the CNT/PDMS-SA, and finally a power meter (EXFO, FPM-300) is used for measuring the transmitted optical power. It is noted that, to avoid any possible Kerr effect induced by the optical coupler and different responses by two power meters, here, balanced twin-detector method is not used. Instead, a highly repeatable electrically tunable optical variable attenuator and only one power meter is used. Before testing the transmission curve, the transmission curve without CNT/PDMS-SA is measured as the background. The measured experimental result is shown in Fig. 7(b). As the injected optical power increases from 0 to 0.5 mW, the transmission of the CNT/PDMS-SA gradually increases and reaches a platform finally. The calculated modulation depth of the SA is about 1 %. The modulation depth plays an important role for laser mode-locking, and the modulation depth of CNT/PDMS-SA is small owing to the low concentration of CNT in the host polymer. Typically, small modulation depth will cause unstable mode-locking, however, the stable mode-locking can be realized if the laser's configuration is reasonable, including net cavity dispersion, gain/loss, and recovery time of SAs [52–54]. For the transmission curve, after a short platform, when the injected power further increases, the transmission of the CNT/PDMS-SA is slowly decreased. This result indicates there exists both saturable absorption and reverse saturable absorption in the CNT/PDMS we use [55,56]. The measured data of transmission can be well fitted by the equation [57]

$$T = 100 - \alpha_0 / (1 + I/I_s) - \alpha_{ns} - \beta I, \quad (1)$$

where T is the transmission (unit in percentage), α_0 is the saturable absorption coefficient, I is the injected optical intensity, I_s is the saturation power, α_{ns} is non-saturable absorption coefficient and β is the reverse saturable absorption coefficient. In the fitting curve, the α_0 is 2.21, I_s is 7.22 W of peak power, α_{ns} is 58.5 %, and β is 0.032. The R-square value of the fitting curve is 0.988. The reverse saturable absorption of CNT/PDMS may result from the nonlinear scattering [51] and nonlinear refraction caused by thermal effect [51,58] under the pulse laser radiation and will increase the cavity loss when increasing the pump power. However, the laser still supports ultrashort pulses generation owing to the different time scales of saturable absorption and reverse saturable absorption [58]. Additionally, we calculated the peak

power and transmission when the laser is operating at single-wavelength mode-locking at both 1558.9 nm and 1532.6 nm. When operating at 1558.9 nm (pump power of 35 mW, average output power of 0.25 mW), the laser pulse owns a peak power of 7.2 W, and the corresponding transmission of the CNT/PDMS-SA is calculated as 40.1 %; when the wavelength is switched to 1532.6 nm (pump power of 100 mW, average output power of 1.9 mW), the peak power is calculated as 42.7 W, and the corresponding transmission is calculated as 39.8 %.

Therefore, the phenomenon of such a pump-driven mode-locking switching can be well explained as follows: First, with the injected pump increases at low power regime, the dominant saturable absorption helps the laser to mode-lock with self-starting. When the optical power is over the saturated power, the reverse saturable absorption is dominant, therefore increasing the intracavity loss. When intracavity loss increased, the population inversion condition of Er-doped fiber is changed accordingly, resulting in the change of gain profile of [59]. As a result, the gain emission peak around 1560 nm is shifted to around 1530 nm, the mode-locking switching is achieved [43].

Finally, to demonstrate there is no spectral filtering effect caused by the CNT/PDMS, the transmitted optical spectra under both ASE and mode-locked laser (MLL) light source are measured, seen as Fig. 8(a) and (b). The black and red curves show the transmission with and without CNT/PDMS, and the black is the normalized transmission. Under both cases, the CNT/PDMS-SA doesn't show any obvious spectral filtering, the transmission in 1500–1600 nm is almost wavelength independent. Therefore, the mode-locking switching is solely caused by the gain profile of Er-doped fiber change induced by increased intracavity loss, which is brought by the reverse saturable absorption of the CNT/PDMS-SA.

4. Conclusions

In conclusion, we have proposed and demonstrated an all-PM CNT/PDMS mode-locked fiber laser without any filter or attenuator, with pump-power-controlled wavelength switchability. The realization of wavelength switching and dual-wavelength mode-locking in such a concise laser cavity is dependent solely on the injected pump power. The mechanism behind the phenomenon is well explained by the intracavity loss variation induced by the reverse saturable absorption of CNT/PDMS. The proposed laser is an ideal source in biochemical sensing, imaging and wavelength multiplexed dual comb spectroscopy, for its compact size, simple wavelength switching scheme, environmentally stable all-PM-fiber configuration.

Funding

Japan Society for the Promotion of Science [grant numbers

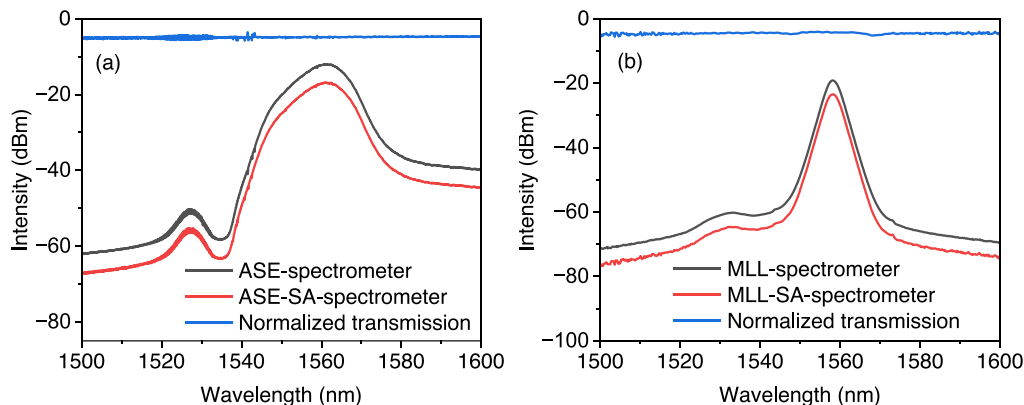


Fig. 8. The transmission curve of the CNT/PDMS using (a) ASE source, and (b) MLL source. (For interpretation of the references to colour in this figure legend, the reader is referred to the web version of this article.)

(22H00209, 23H00174); Core Research for Evolutional Science and Technology (JPMJCR1872).

CRedit authorship contribution statement

Maolin Dai: Writing – original draft, Methodology, Investigation, Formal analysis, Data curation, Conceptualization. **Bowen Liu:** Methodology, Data curation. **Guanyu Ye:** Formal analysis, Data curation. **Takuma Shirahata:** Project administration, Methodology, Formal analysis, Data curation. **Yifan Ma:** Software, Methodology, Investigation, Formal analysis. **Naoki Yamaguchi:** Visualization, Software, Formal analysis. **Sze Yun Set:** Writing – review & editing, Supervision, Funding acquisition. **Shinji Yamashita:** Writing – review & editing, Supervision, Funding acquisition.

Declaration of competing interest

The authors declare that they have no known competing financial interests or personal relationships that could have appeared to influence the work reported in this paper.

Data availability

Data will be made available on request.

Acknowledgement

We thank Mr. Hideru Sato and Mr. Raymond Chen for their kind personal donation for this research work.

References

- J. Kim, Y.J. Song, Ultralow-noise mode-locked fiber lasers and frequency combs: principles, status, and applications, *Adv. Opt. Photon.* 8 (2016) 465–540.
- Y. Han, Y.B. Guo, B. Gao, C.Y. Ma, R.H. Zhang, H. Zhang, Generation, optimization, and application of ultrashort femtosecond pulse in mode-locked fiber lasers, *Prog. Quantum Electron.* 71 (2020).
- M.E. Fermann, I. Hartl, Ultrafast fibre lasers, *Nat. Photonics* 7 (2013) 868–874.
- V.J. Matsas, W.H. Loh, D.J. Richardson, Self-strating, passively mode-locked Fabry-Perot fiber soliton laser using nonlinear polarization evolution, *IEEE Photon. Technol. Lett.* 5 (1993) 492–494.
- Z.Y. Yan, X.H. Li, Y.L. Tang, P.P. Shum, X. Yu, Y. Zhang, Q.J. Wang, Tunable and switchable dual-wavelength Tm-doped mode-locked fiber laser by nonlinear polarization evolution, *Opt. Express* 23 (2015) 4369–4376.
- V.J. Matsas, D.J. Richardson, T.P. Newson, D.N. Payne, Characterization of a self-starting, passively mode-locked fiber ring laser that exploits nonlinear polarization evolution, *Opt. Lett.* 18 (1993) 358–360.
- M. Edelmann, Y. Hua, K. Safak, F.X. Kärtner, Intrinsic amplitude-noise suppression in fiber lasers mode-locked with nonlinear amplifying loop mirrors, *Opt. Lett.* 46 (2021) 1752–1755.
- M. Michalska, Dispersion managed thulium-doped fiber laser mode-locked by the nonlinear loop mirror, *Opt. Laser Technol.* 138 (2021).
- Y. Han, H.C. Tian, F. Meng, K. Wang, S.Y. Cao, Environment-stable sub-100 fs Er: fiber laser with a 3 dB bandwidth of 78 nm, *Opt. Express* 30 (2022) 48021–48029.
- A.S. Mayer, W. Grosinger, J. Fellingner, G. Winkler, L.W. Perner, S. Droste, S. H. Salman, C. Li, C.M. Heyl, I. Hartl, O.H. Heckl, Flexible all-PM NALM Yb: fiber laser design for frequency comb applications: operation regimes and their noise properties, *Opt. Express* 28 (2020) 18946–18968.
- D. Kim, D. Kwon, B. Lee, J. Kim, Polarization-maintaining nonlinear-amplifying-loop-mirror mode-locked fiber laser based on a 3 x 3 coupler, *Opt. Lett.* 44 (2019) 1068–1071.
- G.Y. Ye, K.K. Chow, B.W. Liu, M.L. Dai, Y.F. Ma, T. Shirahata, S. Yamashita, S. Y. Set, L-band mode-locked fiber laser using all polarization-maintaining nonlinear polarization rotation, *Opt. Lett.* 48 (2023) 4729–4732.
- X.Y. Liu, Q. Li, D.H. Pan, F. Ye, B. Malomed, H.Y. Fu, A robust and novel linear fiber laser mode-locked by nonlinear polarization evolution in all-polarization-maintaining fibers, *J. Lightwave Technol.* 39 (2021) 7509–7516.
- J. Szczepanek, T. M. Kardas, C. Radzewicz, and Y. Stepanenko, “Ultrafast laser mode-locked using Nonlinear Polarization Evolution in Polarization Maintaining fibers,” in *Conference on Lasers and Electro-Optics (CLEO)*(San Jose, CA, 2017).
- Y.H. Shi, Z.G. Peng, Z.C. Cheng, T. Xia, H. Zhao, S.Q. Wan, P. Wang, All-fiber polarization-maintaining dispersion-managed figure-of-9 mode-locked laser, *IEEE Photon. Technol. Lett.* 34 (2022) 251–254.
- Q.H. Deng, K. Yin, J.H. Zhang, X. Zheng, T. Jiang, A 200 MHz compact environmentally-stable mode-locked figure-9 fiber laser, *IEEE Photonics J.* 13 (2021).
- I.A. Litago, D. Leandro, M.A. Quintela, R.A. Pérez-Herrera, M. López-Amo, J. M. López-Higuera, Tunable SESAM-based mode-locked soliton fiber laser in linear cavity by axial-strain applied to an FBG, *J. Lightwave Technol.* 35 (2017) 5003–5009.
- J. Boguslawski, L. Sterczewski, D. Stachowiak, G. Sobon, Intracavity filtering in SESAM mode-locked fiber lasers: soliton effects and noise performance, *Opt. Express* 31 (2023) 27667–27676.
- S.Y. Set, H. Yaguchi, Y. Tanaka, M. Jablonski, Laser mode locking using a saturable absorber incorporating carbon nanotubes, *J. Lightwave Technol.* 22 (2004) 51–56.
- S. Yamashita, Y. Inoue, S. Maruyama, Y. Murakami, H. Yaguchi, M. Jablonski, S. Y. Set, Saturable absorbers incorporating carbon nanotubes directly synthesized onto substrates and fibers and their application to mode-locked fiber lasers, *Opt. Lett.* 29 (2004) 1581–1583.
- Q.L. Bao, H. Zhang, Y. Wang, Z.H. Ni, Y.L. Yan, Z.X. Shen, K.P. Loh, D.Y. Tang, Atomic-layer graphene as a saturable absorber for ultrafast pulsed lasers, *Adv. Funct. Mater.* 19 (2009) 3077–3083.
- Z.P. Sun, T. Hasan, F. Torrisi, D. Popa, G. Privitera, F.Q. Wang, F. Bonaccorso, D. M. Basko, A.C. Ferrari, Graphene mode-locked ultrafast laser, *ACS Nano* 4 (2010) 803–810.
- J. Lee, J. Koo, Y.M. Jhon, J.H. Lee, A femtosecond pulse erbium fiber laser incorporating a saturable absorber based on bulk-structured Bi₂Te₃ topological insulator, *Opt. Express* 22 (2014) 6165–6173.
- J. Sotor, G. Sobon, W. Macherzynski, P. Paletko, K. Grodecki, K.M. Abramski, Mode-locking in Er-doped fiber laser based on mechanically exfoliated Sb₂Te₃ saturable absorber, *Optical Materials Express* 4 (2014) 1–6.
- S.X. Wang, H.H. Yu, H.J. Zhang, A.Z. Wang, M.W. Zhao, Y.X. Chen, L.M. Mei, J. Y. Wang, Broadband few-layer MoS₂ saturable absorbers, *Adv. Mater.* 26 (2014) 3538–3544.
- H. Zhang, S.B. Lu, J. Zheng, J. Du, S.C. Wen, D.Y. Tang, K.P. Loh, Molybdenum disulfide (MoS₂) as a broadband saturable absorber for ultra-fast photonics, *Opt. Express* 22 (2014) 7249–7260.
- J. Sotor, G. Sobon, M. Kowalczyk, W. Macherzynski, P. Paletko, K.M. Abramski, Ultrafast thulium-doped fiber laser mode locked with black phosphorus, *Opt. Lett.* 40 (2015) 3885–3888.
- K. Park, J. Lee, Y.T. Lee, W.K. Choi, J.H. Lee, Y.W. Song, Black phosphorus saturable absorber for ultrafast mode-locked pulse laser via evanescent field interaction, *Ann. Phys.* 527 (2015) 770–776.
- X.T. Jiang, S.X. Liu, W.Y. Liang, S.J. Luo, Z.L. He, Y.Q. Ge, H.D. Wang, R. Cao, F. Zhang, Q. Wen, J.Q. Li, Q.L. Bao, D.Y. Fan, H. Zhang, Broadband nonlinear photonics in few-layer MXene Ti₃C₂T_x (T = F, O, or OH), *Laser Photonics Rev.* 12 (2018).
- Y.I. Jhon, J. Koo, B. Anasori, M. Seo, J.H. Lee, Y. Gogotsi, Y.M. Jhon, Metallic MXene saturable absorber for femtosecond mode-locked lasers, *Adv. Mater.* 29 (2017).
- K.Y.T. Lee, S.Y. Kwon, T. Woo, J. Ryu, J.H. Jung, J.H. Lee, Nonlinear absorption and refraction properties of V₄C₃ MXene and its use for an ultra-broadband saturable absorber, *Adv. Opt. Mater.* 11 (2023).
- K. Lee, I.H. Lee, Y.G. Khim, S.Y. Kwon, G. Lim, J. Jung, Y.J. Chang, J.H. Lee, Nonlinear optical properties of PVD-grown Cr₂Te₃ film and its nonlinear switching application, *J. Alloy. Compd.* 956 (2023).
- N.N. Xu, S. Sun, X.X. Shang, H.N. Zhang, D.W. Li, Harmonic and fundamental-frequency mode-locked operations in an Er-doped fiber laser using a Cr₂Si₂Te₆-based saturable absorber, *Optical Materials Express* 12 (2022) 166–173.
- Z. Kang, Q. Li, X.J. Gao, L. Zhang, Z.X. Jia, Y. Feng, G.S. Qin, W.P. Qin, Gold nanorod saturable absorber for passive mode-locking at 1 μm wavelength, *Laser Phys. Lett.* 11 (2014).
- C.H. Zhu, F.Q. Wang, Y.F. Meng, X. Yuan, F.X. Xiu, H.Y. Luo, Y.Z. Wang, J.F. Li, X. J. Lv, L. He, Y.B. Xu, J.F. Liu, C. Zhang, Y. Shi, R. Zhang, S.N. Zhu, A robust and tuneable mid-infrared optical switch enabled by bulk Dirac fermions, *Nat. Commun.* 8 (2017).
- J.S. He, L.L. Tao, H. Zhang, B. Zhou, J.B. Li, Emerging 2D materials beyond graphene for ultrashort pulse generation in fiber lasers, *Nanoscale* 11 (2019) 2577–2593.
- X. Sun, Y. Zhu, L. Jin, S. Yamashita, S.Y. Set, Polarization-maintaining all-fiber tunable mode-locked laser based on a thermally controlled Lyot filter, *Opt. Lett.* 47 (2022) 4913–4916.
- M.L. Dai, B.W. Liu, T. Shirahata, X.N. Sun, S.Y. Set, S. Yamashita, All-polarization-maintaining, efficiently wavelength-tunable, Er-doped mode-locked fiber laser with a compact reflective Lyot filter, *Opt. Express* 31 (2023) 27810–27820.
- Z.R. Li, N. Lv, X. Feng, S. Li, Y.Y. Sun, Y. Yin, P.F. Wang, C-band dual-wavelength synchronized mode-locked erbium-doped fiber laser using a common absorber, *Opt. Commun.* 542 (2023).
- K.Y. Lau, M.H. Abu Bakar, F.D. Muhammad, A.A. Latif, M.F. Omar, Z. Yusoff, M. A. Mahdi, Dual-wavelength, mode-locked erbium-doped fiber laser employing a graphene/poly(methyl-methacrylate) saturable absorber, *Opt. Express* 26 (2018) 12790–12800.
- H.G. Rosa, D. Steinberg, E.A.T. de Souza, Explaining simultaneous dual-band carbon nanotube mode-locking Erbium-doped fiber laser by net gain cross section variation, *Opt. Express* 22 (2014) 28711–28718.
- C. Zeng, Y.D. Cui, J. Guo, Observation of dual-wavelength solitons and bound states in a nanotube/microfiber mode-locking fiber laser, *Opt. Commun.* 347 (2015) 44–49.
- X. Zhao, Z. Zheng, L. Liu, Y. Liu, Y.X. Jiang, X. Yang, J.S. Zhu, Switchable, dual-wavelength passively mode-locked ultrafast fiber laser based on a single-wall carbon nanotube modelocker and intracavity loss tuning, *Opt. Express* 19 (2011) 1168–1173.

- [44] J.H. Kim, J.Y. Hwang, H.R. Hwang, H.S. Kim, J.H. Lee, J.W. Seo, U.S. Shin, S. H. Lee, Simple and cost-effective method of highly conductive and elastic carbon nanotube/polydimethylsiloxane composite for wearable electronics, *Sci. Rep.* 8 (2018).
- [45] W.J. Tomlinson, R.H. Stolen, C.V. Shank, Compression of optical pulses chirped by self-phase modulation in fibers, *Journal of the Optical Society of America B-Optical Physics* 1 (1984) 139–149.
- [46] J. Jeon, J. Lee, J.H. Lee, Numerical study on the minimum modulation depth of a saturable absorber for stable fiber laser mode locking, *Journal of the Optical Society of America B-Optical Physics* 32 (2015) 31–37.
- [47] X. Luo, T.H. Tuan, T.S. Saini, H.P.T. Nguyen, T. Suzuki, Y. Ohishi, Tunable and switchable all-fiber dual-wavelength mode locked laser based on Lyot filtering effect, *Opt. Express* 27 (2019) 14635–14647.
- [48] X.W. Zhou, Z.C. Cheng, Y.H. Shi, H.D. Guo, P. Wang, High-Energy Noiselike Pulses in an all-PM Double-Clad Er/Yb-Codoped Fiber Laser, *IEEE Photon. Technol. Lett.* 30 (2018) 985–988.
- [49] G.Q. Hu, L.Q. Zhu, G.K. Sun, L.L. Lu, R. You, Y. Liu, W. He, M.L. Dong, Spectral overlapping single-cavity dual-comb fiber laser with well-controlled repetition rate difference, *Appl. Phys. Lett.* 121 (2022).
- [50] M.L. Dennis, I.N. Duling, Experimental-study of side-band generation in femtosecond fiber lasers, *IEEE J. Quantum Electron.* 30 (1994) 1469–1477.
- [51] L. Vivien, P. Lançon, D. Riehl, F. Hache, E. Anglaret, Carbon nanotubes for optical limiting, *Carbon* 40 (2002) 1789–1797.
- [52] J.H. Yim, W.B. Cho, S. Lee, Y.H. Ahn, K. Kim, H. Lim, G. Steinmeyer, V. Petrov, U. Griebner, F. Rotermund, Fabrication and characterization of ultrafast carbon nanotube saturable absorbers for solid-state laser mode locking near 1 μm , *Appl. Phys. Lett.* 93 (2008).
- [53] H. Jeong, S.Y. Choi, F. Rotermund, K. Lee, D.I. Yeom, All-polarization maintaining passively mode-locked fiber laser using evanescent field interaction with single-walled carbon nanotube saturable absorber, *J. Lightwave Technol.* 34 (2016) 3503–3507.
- [54] J. Lee, S. Kwon, J.H. Lee, Numerical investigation of the impact of the saturable absorber recovery time on the mode-locking performance of fiber lasers, *J. Lightwave Technol.* 38 (2020) 4124–4132.
- [55] D.J. Harter, Y.B. Band, E.P. Ippen, Theory of mode-locked lasers containing a reverse saturable absorber, *IEEE J. Quantum Electronics* 21 (1985) 1219–1228.
- [56] S. Yamashita, Nonlinear optics in carbon nanotube, graphene, and related 2D materials, *APL Photonics* 4 (2019).
- [57] G. Wang, Y. Ma, C. Shang, H. Huang, Z. Lu, S. Wang, J. Sun, C. Zhang, B. Fu, Influence of reverse saturable absorption effect on conventional and dissipative solitons fiber lasers, *Opt. Laser Technol.* 137 (2021).
- [58] R. Ishida, T.S.L. Prugger Suzuki, S. Fujii, T. Tanabe, The influence of reverse saturable absorption of SWCNTs on mode locking in a fiber-ring resonator, in: *Frontiers in Optics + Laser Science APS/DLS*, Optica Publishing Group, Washington, DC, 2019.
- [59] P.M. Becker, A.A. Olsson, J.R. Simpson. Erbium-doped fiber amplifiers: fundamentals and technology, Elsevier Academic Press, 1999.